

Structure and Symmetry in Coherent Perfect Polarization Rotation

Michael Crescimanno,* Chuanhong Zhou, James H. Andrews, Michael A. Baker

Department of Physics and Astronomy, Youngstown State University, Youngstown, OH 44555-2001, USA*

(Dated: November 27, 2024)

Theoretical investigations of different routes to coherent perfect polarization rotation illustrate its phenomenological connection with coherent perfect absorption. Studying systems with broken parity, layering, combined Faraday rotation and optical activity, or a rotator-loaded optical cavity highlights their similarity and suggests new approaches to improving and miniaturizing optical devices.

PACS numbers: 42.25.Bs, 78.20.Ls, 42.25.Hz, 78.67.Pt

I. INTRODUCTION

Coherent perfect polarization rotation (or CPR) [1] is a conservative, reversible example of a multiport, maximally efficient, optical mode conversion process. As such it shares phenomenological correspondences with the coherent perfect absorber (antilaser or CPA) [2, 3] which has been well studied [4–7]. While many optical devices such as laser wavelength locks, field sensors, optical isolators, and modulators are based on the non-reciprocal nature of Faraday rotation, one way to improve all of these devices is to process all of the incident light coherently. CPR-based design is an intrinsically multi-(input)port approach that combines the non-reciprocal nature of the Faraday effect with interference to convert *all* of the incident light into its orthogonal polarization. An example of the basic two-port CPR device is shown in Fig. 1.

For the apparatus shown in Fig. 1, one still must tune the magnetic field to specific values to achieve complete conversion of the polarization. The required field is sig-

nificantly below that of a single port rotator, however. For one example, the complete conversion of one polarization into the orthogonal polarization using an uncoated terbium gallium garnet (TGG) slab requires only 60% of the field-length product needed for the same rotation in just transmitted light [1]. Achieving complete polarization conversion at a lower field-length product is technologically useful because it is precisely the seeming “incompressibility” of this product and the modest Verdet coefficients of commercially available optical materials that pose a major obstacle to the diffusion of single port designs into integrated optical assemblies and low cost devices. The primary motivation for the work reported here is to quantify in typical one-dimensional optical geometries how CPR-based optical design significantly lowers the field-length product. We characterize the reduction of the threshold field-length product at which coherent perfect processes first occur consequent to specific design choices in optical dispersion, structural dispersion, broken parity, and localization.

A second motivation for this study is to reveal general principles common among coherent perfect processes. Enlarging the context for these phenomena builds intuition useful for finding routes to improving optical devices. We do this primarily by comparing and contrasting CPR and CPA. Note that in both CPR and CPA, a tunable time-odd optical process (magneto-optical rotation for CPR versus absorption in CPA) is combined with multiport wave interference to achieve perfectly efficient mode conversion (to orthogonal polarization in CPR and to electronic excitation in CPA). Among other commonalities between CPA and CPR are their critical dependence on the relative optical phases among the input lightfields. As in the single port case of critical coupling, CPA and CPR both require a particular (hereafter “threshold”) magnitude for the time-odd process. In both CPR and CPA the conversion efficiency has a resonance-like structure. Also, for a fixed wavelength going both above or below threshold makes complete conversion impossible. Because this “resonance” is not associated with a particular decay timescale, coherent perfect resonances are intrinsically zero-width.

Understanding of coherent perfect absorption (CPA) phenomena in diverse optical systems has advanced steadily. Theory relates CPA states to self-dual spectral

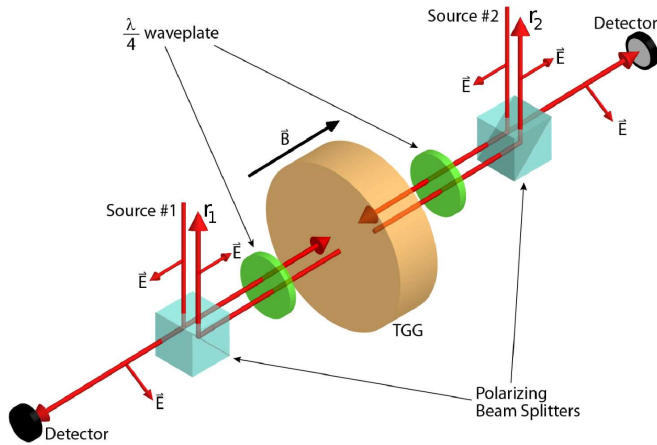


FIG. 1. Basic schematic of two-port CPR device. Not shown are attenuators and delay plates that balance the input field’s amplitude and phase. When the CPR resonance condition is achieved, the reflected light r_1 and r_2 vanishes.

* dcphnt@gmail.com

singularities [2, 8] of the S-matrix. The CPA threshold's dependence on the depth of the sample is well understood theoretically, and this dependence has been modeled in complex (but still linear) media such as gold-silica composites and other plasmonic systems [9, 10], and nonlinear media [11]. Both ordinary and \mathcal{PT} -symmetric systems elicit a diverse set of CPA phenomena with those most relevant to CPA thresholds including gratings [12–15], surface plasmonic polaritons [16], photonic crystals [17], near-zero- ϵ materials [18], cavities with absorbers [19], controlled disorder or other spatial ordering [20, 21], and very thin absorptive layers [22]. Some of these ideas are also being explored for technological uses including all optical switching [23–27] and CPA enhancement of photoluminescence [28].

After fixing notation and giving a brief review of the basic phenomena, Section III explores CPR and contrasts it with CPA in different optical environments, highlighting the roles played by dispersion, parity, and transport of mixed symmetry type. In Section IIIA we focus on coherent perfect phenomena in model multilayer systems, followed in Section IIIB by breaking parity two different ways (first softly with randomness and then explicitly with trinary multilayers). Thematically up to that point, one sees a direct correspondence between the layering effects on CPR and CPA states and thresholds. Subtle differences between the two are discussed in one archetypal example combining CPR and optical rotation in Section IIIC. A brief conclusion highlights new directions prompted by this study.

II. NOTATION AND PRELIMINARIES

We use matrices to represent linear transport and work in the basis where the local field (complex) amplitudes for light traveling along the \hat{z} -axis are $\vec{v} = (E_x, H_y, E_y, -H_x)$. In terms of the individual polarization and motional states, we use $\vec{e}_R = (E_x, H_y) = (1, 1)$ for a right-moving wave and $\vec{e}_L = (-1, 1)$ for a left-moving one. Throughout this paper we restrict ourselves to materials without linear birefringence (in contrast with [29]) The $O(2)$ symmetry about the axial direction implies for the transport $\vec{v}_{i+1} = \mathcal{M}_i \vec{v}_i$ that the 4×4 \mathcal{M} can be written (in this basis) in terms of the 2×2 's M and C as $\mathcal{M} = \begin{pmatrix} M & C \\ -C & M \end{pmatrix}$, where C is only nonzero for transport that mixes the polarization states.

For dielectrics (also the only case we consider below), the matrix M is proportional to the familiar 2×2 transfer matrix for the individual polarizations. For example, for a unit intensity wave incident from the left, in steady state, the field amplitudes at the surface are $\vec{e}_{\text{in}} = (1, 1) + r(-1, 1)$, where r is the reflected amplitude. The outgoing field amplitude to the right of the system is given via $\vec{e}_{\text{out}} = t(1, 1) = M\vec{e}_{\text{in}}$, where t is the transmission amplitude. In this basis, for a purely

dielectric material of thickness L , index n ,

$$M = \begin{bmatrix} \cos \delta & \frac{i}{n} \sin \delta \\ in \sin \delta & \cos \delta \end{bmatrix}, \quad (1)$$

where $\delta = nk_0L$ and k_0 is the vacuum wavenumber. Note that $\det(M) = 1$ always, but M_{11} and M_{22} are only equal in systems that have overall spatial parity symmetry. We identify the real part of the index n with refraction and its positive/negative imaginary part with absorption/gain.

Analytically for a slab dielectric Faraday rotator the M and C parts of the \mathcal{M} in our field basis are [1, 30]

$$M = \frac{1}{2} \begin{bmatrix} C_1 + C_2 & i(S_1/n_1 + S_2/n_2) \\ i(n_1 S_1 + n_2 S_2) & C_1 + C_2 \end{bmatrix} \quad (2)$$

and

$$C = \frac{1}{2} \begin{bmatrix} i(C_1 - C_2) & -(S_1/n_1 - S_2/n_2) \\ -(n_1 S_1 - n_2 S_2) & i(C_1 - C_2) \end{bmatrix}, \quad (3)$$

where $C_{1,2}$ ($S_{1,2}$) refer to the cosine (sine) of $\delta_{1,2} = n_{1,2}k_0L$ in which the n_1, n_2 are the indices of refraction of the left- and right- circular polarization in the slab, k_0 refers to the vacuum wavevector, and L is the thickness of the slab. For a dielectric slab in an external magnetic field pointing along the direction of propagation, $\Delta n = n_1 - n_2 \propto VB$, the product of the Verdet and the magnetic field. Note that the resulting 4×4 matrix \mathcal{M} is quite different from one representing optical activity (a time-even rotation process) which has the form $M = \cos \alpha M_0$ and $C = \sin \alpha M_0$, where α is proportional to the density of chiral centers in the slab and M_0 is the usual 2×2 transfer matrix given by Eq. (1). Because CPR is a reversible optical process we require constant local power flux throughout in steady state. This condition thus requires the n 's and the α to be real throughout for both the time-even and time-odd rotation processes we consider below.

For a single polarization whose linear transport is given entirely in terms of a net 2×2 transfer matrix M in the basis described above and used throughout, the CPA state is reached when the condition $(1, 1)M(1, 1)^t = M_{11} + M_{12} + M_{21} + M_{22} = 0$ is satisfied. For a general 2×2 matrix, this condition combined with the determinant indicates that CPA implies four real conditions for four complex numbers. A remaining freedom of optical field (amplitude and phase) then implies that CPA requires, at minimum, tuning two dimensionless experimental parameters, typically, the ratio L/λ and the absorptive index $Im(n)$.

It is also straightforward to find the condition associated with CPR resonances using the 4×4 basis. For fields incident from the left, take $\vec{v}_l = (1, 1, -l, l)$, where l is the amplitude of the reflected, rotated wave. On the right, take $\vec{v}_r = (-d, d, s, s)$; this configuration thus consists of incoming fields of one polarization and outgoing fields of the orthogonal polarization only, the CPR state. In analogy with the CPA state, these boundary conditions lead

to a condition on the size, wavelength and rotary power of the system. For CPR resonance in uniaxial systems with the 4×4 form of \mathcal{M} as described earlier, we require

$$M \begin{pmatrix} 1 \\ 1 \end{pmatrix} + C \begin{pmatrix} -1 \\ 1 \end{pmatrix} l = \begin{pmatrix} -1 \\ 1 \end{pmatrix} d \quad (4)$$

and

$$-C \begin{pmatrix} 1 \\ 1 \end{pmatrix} + M \begin{pmatrix} -1 \\ 1 \end{pmatrix} l = \begin{pmatrix} 1 \\ 1 \end{pmatrix} s. \quad (5)$$

Counting conditions (four complex) for the three complex fields (d, l, s), we see that to achieve CPR by simultaneously solving Eqs. (4) and (5) requires, at minimum, tuning two experimental parameters (here, generically, the ratio L/λ and the circular birefringence $\Delta n = n_1 - n_2$), which we note is analogous to the CPA case (where the parameters are (L/λ) and the absorption coefficient). Eliminating the fields d, l, s , we can write the CPR condition succinctly for a general \mathcal{M} as a single complex condition $\det(R) = 0$, where the 2×2 matrix R has the following elements:

$$R_{11} = (-1, 1)C^{-1}M \begin{pmatrix} -1 \\ 1 \end{pmatrix} \quad (6)$$

$$R_{12} = -(-1, 1)C^{-1} \begin{pmatrix} 1 \\ 1 \end{pmatrix} \quad (7)$$

$$R_{21} = (1, 1)[MC^{-1}M + C] \begin{pmatrix} -1 \\ 1 \end{pmatrix} \quad (8)$$

$$R_{22} = -(1, 1)MC^{-1} \begin{pmatrix} 1 \\ 1 \end{pmatrix}. \quad (9)$$

We now summarize CPR phenomenology in a series of optical systems in order to build a deeper intuition about the CPR state and its connection to and contrast with CPA, with an eye towards its potential utility in optical devices.

III. CPR IN MODEL SYSTEMS

A. CPR in layered binary systems

Studying CPR in multilayer interference films provides a straightforward comparison of CPR and CPA phenomena and their dependence on dispersion, both material and structural. For simplicity, consider first a perfectly periodic multilayer composed of N alternating layers of a material A that is a dielectric with zero Verdet and a material B that has a non-zero Verdet. We compare these systems to the CPA model system in which the bilayers have one non-absorbing species (A) and the other absorbing (B). In all the model systems described here, only

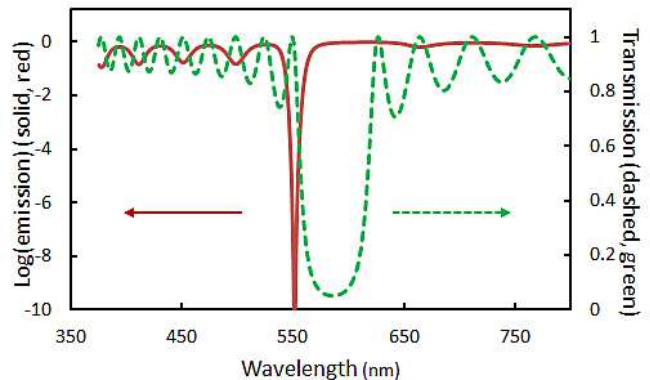


FIG. 2. (Color online) Typical CPR resonance in a 1-d photonic crystal. The green dashed trace is the transmission trace and the red solid trace is the total output light in the same polarization as the input polarization. This example is 31 alternating layers (each 100 nm thick) of index 1.55 (non Faraday) and 1.38 (Faraday), corresponding to the first row in Table I [31]. Clearly seen in the dashed green trace is the reflection bandgap that extends from 550-625 nm. The CPR resonance is the pronounced reduction in the output light polarized along the input polarization for wavelengths near the short wavelength edge of the band.

TABLE I. CPR thresholds (Δn values for the circular polarization propagation eigenstates in layer B) at the reflection band edge for the layered binary systems described in Fig. 2. Throughout this paper the letters after the threshold values indicate the spatial symmetry (O for odd, E for even) of that CPR resonance's fields.

configuration	31 layers	33 layers
$n_A > n_B$.049(E)	.044(O)
$n_A < n_B$.090(E)	.080(O)

the B species rotates (for CPR) or absorbs (for CPA). The species have different indices of refraction in the absence of a magnetic field (for CPR) or absorption (for CPA) that we denote n_A and n_B , creating an optical (reflection) bandgap. We denote these layered systems as $(AB)^N$, but here, to eliminate any spurious effect from explicitly broken parity, we restrict our attention to parity symmetric layered systems formed by adding one terminal A layer, that is, $(AB)^N A$.

One finding of these simulations (see Fig. 2) is that for the lowest thresholds, layered films with an odd number of bilayers (*e.g.*, 31 layers) had threshold CPR states of even parity and those with an even number of bilayers (*e.g.*, 33 layers) had threshold CPR states of odd parity. A simple explanation of this observation is given in the next subsection on consequences of parity symmetry (and parity breaking).

Note also that the wavelength at which the lowest CPR resonance occurs is at a band edge. As is well known, across the reflection bandgap there is pronounced optical dispersion resulting in large increases in the group

velocity delay symmetrically at the band edges, and significant reductions in the delay in the middle of the band. (Ref.[32] is a recent relevant summary.) The reduction in the threshold for CPR/CPA with increases in group velocity delay at the band edge is most clearly seen by plotting the product of the threshold value of the rotary power of the B layers times the number of layers versus the number of layers, as in Fig. 3 (dashed green trace) which hews closely to a plot of the group velocity minima versus the number of layers (solid red trace).

Changes in the group velocity delay are, in and of themselves, not enough to explain the pattern of CPR (and CPA) resonances in these systems; the lowest threshold for the CPR/CPA resonances for $n_A > n_B$ occurs at the short wavelength side of the bandgap but occurs at the long wavelength edge of the bandgap for $n_A < n_B$. As the time reverse of CPA, actual lasing [33], indicates, the simplest way to explain this difference is by apportioning the group velocity delay across the two species of the multilayer, and noting that only in the B species is the light subject to polarization rotation (CPR) or absorption/gain (CPA/lasing). Simulations of the local electric field of the light traversing the multilayer indicate that, off-band, the apportionment of the total velocity delay should follow the ratio of the indices. Near the long wavelength side of the band edge, however, the light's integrated electric energy is greater in the larger index species, whereas the reverse occurs at the short wavelength edge of the bandgap [34]. Equating field energy to the probability that the light visits that species, and apportioning part of the total propagation time (and thus the overall Faraday rotation) to each species in proportion to that probability, qualitatively explains both the wavelength and the threshold of the CPR/CPA resonances.

Just as in CPA, there are other CPR states that arise at different wavelengths as one increases Δn beyond threshold. Note that for these simple binary multilayers, the next-to-lowest CPR resonance typically occurs at the opposite band edge, as expected and formerly noted [12] for CPA. To summarize the results from this study of CPR in multilayers in experimental terms, a 0.76 mm thick multilayer of 160 nm layers of each Bismuth-substituted iron garnet (called "BIG", index of refraction of ~ 2.3 at 633 nm, at which the Verdet is $\sim -7 \times 10^3$ rad/Tm [30]) and ordinary SiO_2 glass would achieve CPR at 0.5 T, whereas a slab of BIG alone of length 2.4 cm would be needed at this field, indicating in concrete terms the substantial reductions in CPR thresholds associated with photonic bands.

In practice with real multilayer systems, non-ideality typically moves CPR/CPA lowest threshold states from the band edge to defect states in the band gap itself. This is consonant with the experience in lasing where it is well documented that layer nonuniformity and other perturbations cause lasing to occur first through defect states typically located within the band gap itself. The defect states still correspond to maxima of the group ve-

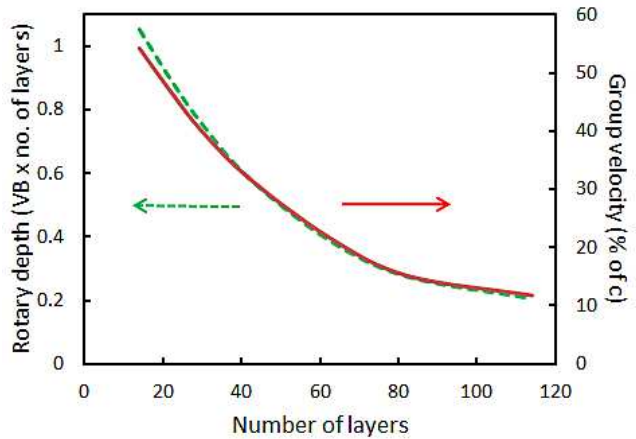


FIG. 3. (Color online) The correspondence between the group velocity delay and the CPR thresholds in layered media. Varying the number of layers only, we plot the product of the CPR threshold Verdet-field (VB) product times the number of layers versus the number of layers. We also plot the group velocity minimum at the band edge versus the number of layers (right axis, solid red trace).

locity delay [35]. (See the discussion of parity breaking in subsection B below.)

It is illustrative to explicitly compare thresholds for lasing/CPA and CPR in simple multilayer systems with deliberate structural defects, such as the "phase-slip" (sometimes called "folded") distributed feedback (DFB) systems [34, 36]. Here we compare the multilayers $(AB)^N(BA)^N$ and $(BA)^N(AB)^N$, where the time-odd process (either Faraday rotation in the case of CPR or absorption/gain in the case of CPA/lasing) is again only in the B -layers. Table II gives calculated threshold Δn values for CPR for four configurations of simply-folded symmetric systems, which agree qualitatively with the corresponding results for CPA/lasing summarized in Fig. 4 (adapted from Ref. [37]). For example, controlling for overall gain, the folded DFB structure with the lowest lasing threshold (as inferred from the largest gain in the figure) is that which has the gain medium in the low index material and is folded on the low index material. This result agrees with our simulations of the CPR threshold as shown in Table II (folded on B , $n_A > n_B$).

For contrast we conclude this section with a case in which dispersion, but not field placement, is important: the loaded optical cavity as a layered optical system. Consider a dielectric Faraday rotator inside an optical cavity composed of transversely isotropic perfectly thin mirrors of reflectivity amplitude r (so that the reflectivity is $R = |r|^2$). The mirrors are represented by the transfer matrix $\mathcal{M}_r = \begin{bmatrix} M_r & 0 \\ 0 & M_r \end{bmatrix}$ where the 2×2 matrices M_r for the simple case of completely non-absorbing mirrors are given in our 'field' basis as $M_r = \frac{1}{\sqrt{1-|r|^2}} \begin{bmatrix} 1 & i|r| \\ -i|r| & 1 \end{bmatrix}$.

TABLE II. The CPR threshold values of Δn for “folded” layered systems comprised of 52 total layers. Every entry in the table is for a CPR resonance occurring on the defect state inside the reflection band. The lowest CPR threshold occurs with even parity when rotation occurs in the lower index material and the fold is on that low index material. The CPR threshold ordering in the chart is in one-to-one agreement with that of lasing thresholds in these “folded” DFB systems reproduced in Fig. 4.

configuration	Fold on A	Fold on B
$n_A > n_B$.032(O)	.013(E)
$n_A < n_B$.017(E)	.028(O)

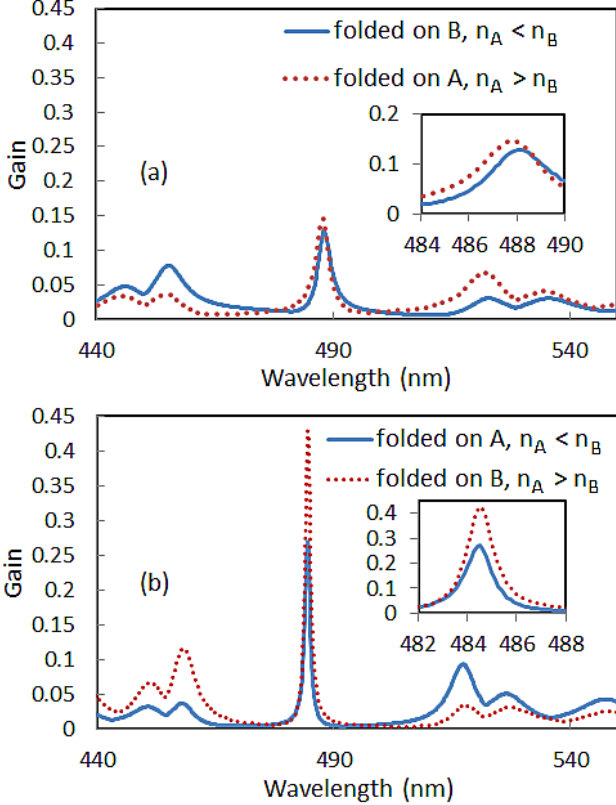


FIG. 4. (Color online) Transmission gain versus wavelength for the folded structures analogous to those in Table II, where instead of rotation in the B -layers a complex index of refraction is used to represent optical gain. In this case the optical band stretched from 450 nm to 520 nm, and the prominent fold defect state appears near the center of the band. (Figure adapted from Ref. [37] with permission of The Optical Society of America.)

Algebra indicates that all effects of the cavity reflectivity modify the conditions for CPR via a single parameter, $\gamma = \frac{2|r|}{1+|r|^2}$. One finds for this loaded cavity configuration (mirror-rotator-mirror) that the CPR condition becomes (compare the $r \rightarrow 0$ limit with Eq.(14) in Ref. [1]):

$$(n_1 + \frac{1}{n_1})S_1C_2 - (n_2 + \frac{1}{n_2})S_2C_1 + \gamma \left(\frac{n_1}{n_2} - \frac{n_2}{n_1} \right) S_1S_2 =$$

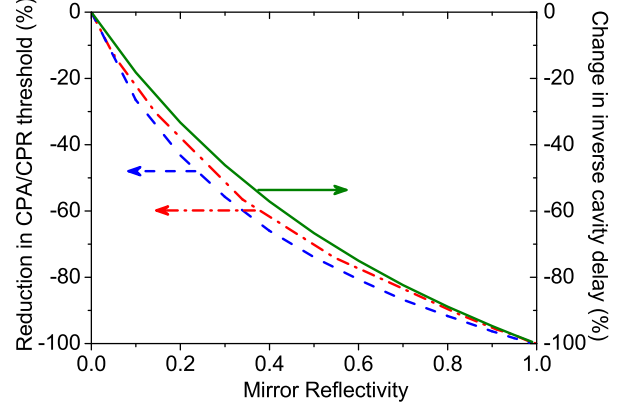


FIG. 5. (Color online) Lowest CPR (red, dot-dash trace) and CPA (blue, dashed trace) resonance thresholds in a loaded cavity decrease as one increases the finesse of the mirrors, going to zero with the inverse of the group velocity delay (green, solid).

$$\pm \left[(n_1 - \frac{1}{n_1})S_1 - (n_2 - \frac{1}{n_2})S_2 + 2\gamma(C_2 - C_1) \right], \quad (10)$$

where, as before, $n_{1,2} = n_0 \pm \Delta n/2$ and $k_0\Delta n = 2VB$.

To compare this result with CPA, it is straightforward to show that the lowest CPA resonance threshold for a cavity loaded with a lossy dielectric modeled as a complex index n is given by the solution of (compare with the $r \rightarrow 0$ limit of Eq. (7) of Ref. [2] also reproduced below in Eq. (13) for completeness):

$$e^{i2nk_0L} = \frac{(n-1)^2 - (n^2+1)\frac{2R}{1+R} + i\gamma(n^2-1)}{(n+1)^2 - (n^2+1)\frac{2R}{1+R} + i\gamma(n^2-1)}. \quad (11)$$

In Fig. 5, we have used Eq. (10) for $n_0 = 2.0$ and $k_0L \sim 820$ to plot the fractional reduction in the lowest CPR resonance threshold (Δn) as a function of the reflectivity, R . The graph shows strong similarity to the inverse of the time spent in the cavity (*i.e.* the fractional reduction in the group velocity), as expected, and also corresponds with the reduction in the CPA threshold of an absorber-loaded cavity shown in the graph. Not included in Fig. 5, we have also analyzed a realistic (*e.g.* complex dielectric) gold mirrored cavity at 780 nm and find qualitatively the same behavior as in Fig. 5 with increasing gold layer thickness. In that study there are no 780 nm CPA states from tuning the loss in the dielectric slab inside the cavity if the gold layer thickness exceeds 35 nm (corresponding to an R of about 85% in each mirror) because at that depth the absorption in the gold itself is above the CPA threshold.

B. CPR with explicitly broken parity

In a parity symmetric absorbing structure, the fields of all CPA states must also be of definite parity, even or

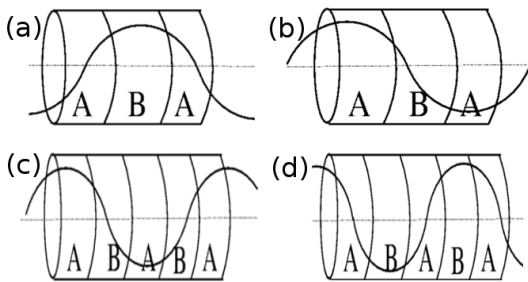


FIG. 6. Parity and CPA/CPR. For an odd number of bilayers, we see that (a) the parity even fields have a maximum on the B species, whereas (b), the parity odd case, the field on the B layer is significantly smaller. For an even number of bilayers, however, the situation is reversed so that (c) parity even fields do not have their maxima on the B layers, but (d) parity odd fields do.

odd. These two possibilities generally occur at different absorption thresholds. Since we have already discussed layered optical systems, one particularly intuitive way to understand this difference is shown in Fig. 6, where one of the species (B) is absorbing (or rotating in the CPR case) and the other species (A) is not. For wavelengths nearly four times the layer thickness (near the band edge) as in the example shown in Fig. 6, the parity even case has larger field overlap on the absorber/rotator (species B) than the parity odd field for an odd number of bilayers (in this case one bilayer), thus the former will have a lower CPA threshold (compare with Table I).

When a rotator (or absorber) is not parity symmetric, there are still CPR (CPA) states, but the state's fields will not be of definite parity. To illustrate the effect of parity breaking on CPR and its comparison with CPA (See Refs. [5, 38]), in this section we consider two examples of parity broken systems: (i) an $(AB)^N A$ multilayer, but with layer-to-layer thickness variations, and (ii) a ternary regular layered system of the type $(ABC)^N$ (in both cases only B is rotary (CPR) or absorptive (CPA)).

As one introduces layer thickness variations into the $(AB)^N A$ structures discussed in the preceding subsection, formerly localized reflection band states mix with extended states whereas some formerly extended states become localized [35]. Initially, weak localization increases the group velocity delay and thus reduces the CPA/CPR threshold for some states near the band edge (see Fig. 7 for one example). As the localization length shrinks further with increasing layer thickness variations, random scattering reduces the coherent band edge reflections that were responsible for the increase in the group velocity delay in the first place. As the level of randomness is increased, the lowest resonant CPR/CPA state's wavelength at threshold moves into what was previously the reflection band. Note also that adding layer thickness randomness explicitly breaks the original parity symmetry of the system. As a consequence, at finite randomness in the CPA case, the amplitude ratio of the input fields is no longer ± 1 .

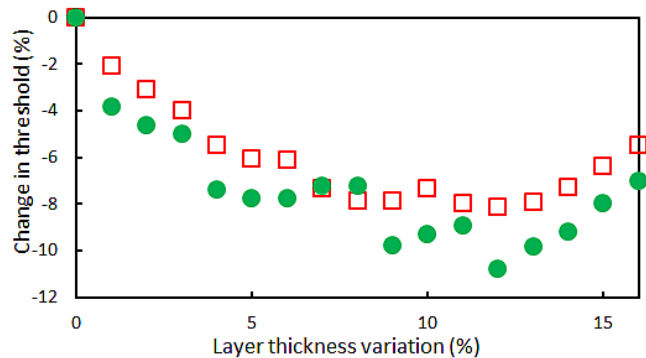


FIG. 7. (Color online) Percentage reduction of CPR (closed circles, green) and CPA (open squares, red) in the thresholds for the lowest CPR/CPA state, which, as described in the text, occur near the band edge. For this example, a particular random layer thickness variation map for the 65 layer multilayer with $n_B > n_A$ (only species B is Faraday (CPR case) or absorptive (CPA case)) is programmed into the simulation and increased across the horizontal axis.

The consequence of parity breaking through broken structural symmetry in CPR is different from that of CPA [39]. Solving Eqs. (4),(5) for the amplitude ratio of the incident fields, l , indicates

$$l = \frac{(M_{11} + M_{12} + M_{21} + M_{22})}{(C_{11} + C_{21} - C_{12} - C_{22})} = \frac{(C_{11} + C_{21} + C_{12} + C_{22})}{(M_{22} + M_{12} - M_{11} - M_{21})} \quad (12)$$

on the CPR state. For any optical system composed of sections without birefringence or optical activity, it was shown in Ref. [1] that the 4×4 \mathcal{M} has underlying 2×2 matrices M and C with the M being time-even and of the form $\begin{bmatrix} \mathcal{R} & \mathcal{I} \\ \mathcal{I} & \mathcal{R} \end{bmatrix}$ and the C being time-odd and of the form $\begin{bmatrix} \mathcal{I} & \mathcal{R} \\ \mathcal{R} & \mathcal{I} \end{bmatrix}$, where \mathcal{R} means a purely real quantity and \mathcal{I} a purely imaginary one. This matrix structure in the formulas for l gives $|l| = 1$, which in turn forces all the optical fields to have the same intensity for a CPR state in any system. The broken parity in the CPR state is instead manifest by the appearance of mismatched phases (not shown) between the input fields.

Explicit parity breaking via structural asymmetry is also evident in the ternary films, $(ABC)^N$, again, in which only B is rotary (CPR) or absorptive (CPA). As an example, Table III shows a comparison of CPR and CPA lowest resonance thresholds near the band edges of the very first reflection band of ternary films. Thus, even for perfectly ordered ternary films, it is the phase mismatch between the left and right input fields that varies universally, while the amplitude ratios only vary for the CPA case. Note also that the threshold values for the cases $n_A > n_C > n_B$ and $n_B > n_A > n_C$ are ordered the

TABLE III. Thresholds for $(ABC)^N$ layered systems where the indices of refraction are chosen from the list $\{1.55, 1.51, 1.38\}$ and the total number of layers is 45 (each layer is 100 nm thick.)

TYPE	configuration	threshold	amplitude ratio
CPR	$n_A > n_C > n_B$.0465	1
CPR	$n_A > n_B > n_C$.0652	1
CPR	$n_B > n_A > n_C$.0752	1
CPA	$n_A > n_C > n_B$.0528	1.44
CPA	$n_A > n_B > n_C$.092	.215
CPA	$n_B > n_A > n_C$.087	1.52

same in both CPR and CPA. In particular, for each of these cases in Table III, the CPR/CPA state forms at the appropriate band edge as discussed in the previous section. The spectral location of the CPR/CPA state in the intermediate case $n_A > n_B > n_C$ depends on the indices' values.

Two additional facts of interest emerge from these simulations. As one might expect, the intensity ratios are more varied for the ternary films (explicit parity breaking) than for the random $(AB)^N A$ layered system (which breaks parity more softly) studied here to only 15% layer thickness variation. Also, for the case of random $(AB)^N A$ layered systems, the variation in the phase is much larger in the CPR case than in the CPA case. Note in this regard that the CPR state forces the intensity ratio to remain unity, whereas for CPA both the amplitude ratio and the phase adjust to stay resonant in a parity broken system.

C. Combined Faraday rotation and optical activity

To highlight the time-reversal symmetries underlying CPR and CPA, we now address the effect that the time-even part of the transport has on the CPR/CPA threshold. In the original derivation of the CPR effect [1] in a simple slab dielectric, increasing the index of refraction of the material reduces the CPR threshold, as shown graphically in Fig. 8 using the formula in Ref. [1]. This is also the case with the CPA threshold, which (see Eq.(7) of Ref. [2]) for an absorbing slab dielectric of index $n = n_0 + in_{abs}$ and length L is:

$$e^{ink_0L} = \pm \frac{(n-1)}{(n+1)}. \quad (13)$$

In the large n_0 limit, because the log is vanishing as $\sim 1/n_0^2$, the threshold n_{abs} must decrease as $\sim 1/n_0$ at large n_0 . A graph of this reduction of CPA in a bulk absorber from Eq. (13) is included in Fig. 9b. We note in passing that this reduction is what one would expect for the single transit time reduction and not that associated with the etaloning as was the case for the optical cavity-assisted reduction in the thresholds.

In CPA, the index of refraction real and imaginary parts can be considered as the time-even and time-odd

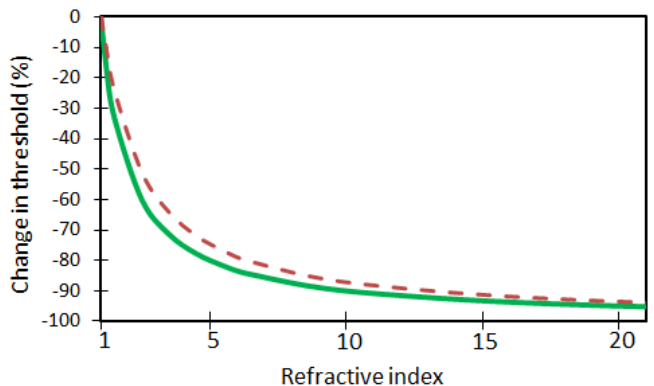


FIG. 8. The CPR threshold reduction (red, dashed) is monotonic to zero as one increases the index of refraction of the slab, following the same relation as in the CPA case ($\sim 1/n$ at large n as described in the text, here as a green, solid line).

contributions to the transport. The analogous processes for the transport of the polarization are optical activity (time-even) and Faraday rotation (time-odd). Recall that one cannot achieve CPR with optical activity alone, but the question we would like to address is how the presence of optical activity in a system modifies the threshold Faraday rotation needed for CPR.

Consider a system with both of these processes operating. Instead of a single bulk piece, for simplicity we analyze a three-layer system composed of two optically active blocks with a Faraday rotator in between. (See discussion below Eq. (1) for the matrix representation of optical activity.) It is then straightforward to identify the CPR state in this system, again in terms of the equation $\det(R) = 0$, where the matrix elements of the 2×2 complex matrix R are as in Eqs. (6)-(9), but where we make the substitutions for M and C via;

$$\begin{pmatrix} M \\ C \end{pmatrix} = \begin{pmatrix} \cos 2\alpha & -\sin 2\alpha \\ \sin 2\alpha & \cos 2\alpha \end{pmatrix} \begin{pmatrix} M_0 M M_0 \\ M_0 C M_0 \end{pmatrix}, \quad (14)$$

where M_0 is given by Eq. (1) for the optically active blocks (with chiral density proportional to α) and the M and C on the RHS of Eq. (14) are given by Eq. (2) and Eq. (3), respectively, for the Faraday block. Keeping the indices and length the same, but changing only the optical activity, we can determine the location of the CPR state (see Fig. 9(a)). We see that, as in the decrease of the CPA threshold with increasing real part of the refractive index n_0 , the Faraday rotation needed to achieve CPR resonance decreases monotonically as one increases the optical rotation in the adjoining slabs. We note that this reduction continues with increasing optical activity beyond the value at which the optical rotary part of the assembly by itself would rotate a single input ray to its orthogonal polarization (rotation by $\pi/2$) upon exiting in transmission. This result is true for both positive and negative Verdet irrespective of the handedness of the optical activity; the trace in Fig. 9(a) is symmet-

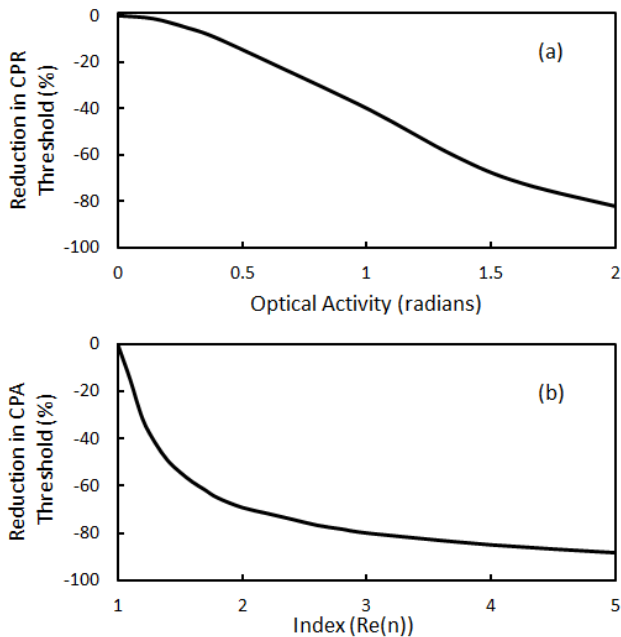


FIG. 9. Lowest CPR and CPA resonance thresholds decrease monotonically to zero as one increases the time-even part of the transport. (a) Reduction in CPR threshold for a Faraday (time odd) constituent sandwiched between two optically active slabs as a function of total optical activity of the time even part standing alone (in radians). (b) Reduction in CPA threshold as a function of the real part of the material's refractive index.

ric about zero optical activity. Both of these (CPR and CPA) curves asymptote to zero threshold. This shows that increasing the time-even part of an optical process reduces the time-odd threshold for achieving CPR/CPA,

and is expected to be useful for reducing the size, complexity and cost of devices based on CPR or CPA, for example by reducing the required magnetic field.

IV. CONCLUSIONS

CPR and CPA are phenomenologically congruent in how their thresholds depend on the system's symmetry, composition and geometry. As both are coherent perfect processes, this congruence follows from the underlying commonality they share through wave interference and discrete symmetry. Furthermore, this study reveals potential design routes to decrease the size and/or magnetic field requirements for achieving CPR. For example, as detailed above, multilayering the rotating species can yield a 30-fold reduction in the naive length-field product. Similarly, even a poor optical cavity with just 60% reflective mirrors reduces the CPR threshold length-field product by nearly 80%. By layering with suitable optically active materials, high index materials, tertiary layered systems and layered systems with small layer thickness variations in the stack, we have shown further reduction in the naive length-field product is achievable in CPR-based devices.

ACKNOWLEDGMENTS

The authors are grateful to the National Science Foundation for financial support under grant number ECCS-1360725 and for financial support from the Science and Technology Center for Layered Polymeric Systems under grant number DMR 0423914.

-
- [1] M. Crescimanno, N. J. Dawson, and J. H. Andrews, *Phys. Rev. A* **86**, 031807(R) (2012).
 - [2] Y. D. Chong, L. Ge, H. Cao, and A. D. Stone, *Phys. Rev. Lett.* **105**, 053901 (2010).
 - [3] W. Wan, Y. Chong, L. Ge, H. Noh, A. D. Stone, and H. Cao, *Science* **331**, 889 (2011).
 - [4] S. Longhi, *Phys. Rev. A* **82**, 031801(R) (2010).
 - [5] Y. D. Chong, L. Ge, and A. D. Stone, *Phys. Rev. Lett.* **106**, 093902 (2011).
 - [6] S. Longhi, *Phys. Rev. Lett.* **107**, 033901 (2011).
 - [7] Z. Lin, H. Ramezani, T. Eichelkraut, T. Kottos, H. Cao, and D. N. Christodoulides, *Phys. Rev. Lett.* **106**, 213901 (2011).
 - [8] A. Mostafazadeh, *Phys. Rev. A* **87**, 012103 (2013).
 - [9] S. Dutta-Gupta, O. J. F. Martin, S. Dutta Gupta, and G. S. Agarwal, *Opt. Express* **20**, 1330 (2012).
 - [10] S. Dutta-Gupta and G. S. Agarwal, *Opt. Lett.* **39**, 390 (2014).
 - [11] S. Longhi, *Phys. Rev. A* **83**, 055804 (2011).
 - [12] Y. Shen, L. Shen, Z. Lai, G. Wang, and X. Deng, *Phys. Lett. A* **378**, 299 (2014).
 - [13] C. Y. Huang, R. Zhang, J. L. Han, J. Zheng, and J. Q. Xu, *Phys. Rev. A* **89**, 023842 (2014).
 - [14] Y. Nakata, Y. Urade, T. Nakanishi, and M. Kitano, *Phys. Rev. B* **88**, 205138 (2013).
 - [15] M. Kang, F. Liu, T.-F. Li, Q.-H. Guo, J. Li, and J. Chen, *Opt. Lett.* **38**, 3086 (2013).
 - [16] X. Luo and L. Yan, *IEEE Photonics J.* **4**, 590 (2012).
 - [17] Z.-R. Zhang, H.-Q. Li, H. Chen, C.-L. Hu, and P. Zhou, *Eur. Phys. Lett.*, **105**, 47008 (2014).
 - [18] S. Feng and K. Halterman, *Phys. Rev. B* **86**, 165103 (2012).
 - [19] K. Egashira, A. Terasaki, and T. Kondow, *Eur. Phys. J. D* **66**, 92 (2012).
 - [20] Y. D. Chong and A. D. Stone, *Phys. Rev. Lett.* **107**, 163901 (2011).
 - [21] L. Ge, Y. D. Chong, S. Rotter, H. E. Tureci, and A. D. Stone, *Phys. Rev. A* **84**, 023820 (2011).
 - [22] M. Pu, Q. Feng, M. Wang, C. Hu, C. Huang, X. Ma, Z. Zhao, C. Wang, and X. Luo, *Opt. Express* **20**, 2246 (2012).

- [23] R. Bruck and O. L. Muskens, *Opt. Express* **21**, 27662 (2013).
- [24] X. Fang, M. L. Tseng, J.-Y. Ou, K. F. MacDonald, D. P. Tsai, and N. I. Zheludev, *Appl. Phys. Lett.* **104**, 141102 (2014).
- [25] R. R. Grote, J. B. Driscoll, and R. M. Osgood, Jr, *Opt. Lett.* **38**, 3001 (2013).
- [26] T. Chen, S. Duan, and Y. C. Chen, *J. Opt. Soc. Am. A* **29**, 689 (2012).
- [27] S. Dutta-Gupta, R. Deshmukh, A. V. Gopal, O. J. F. Martin, and S. Dutta Gupta, *Opt. Lett.* **37**, 4452 (2012).
- [28] G. Pirruccio, G. Lozano, Y. Zhang, S. R. K. Rodriguez, R. Gomes, Z. Hens, and J. G. Rivas, *Phys. Rev. B* **85**, 165455 (2012).
- [29] Y. Wang, M. Pu, C. Hu, C. Hu, Z. Zhao, C. Wang, and X. Luo, *Opt. Commun.*, **319**, 14 (2014).
- [30] H. Kato, T. Matsushita, A. Takayama, M. Egawa, K. Nishimura, and M. Inoue, *J. Appl. Phys.* **93**, 3906 (2003).
- [31] These somewhat arbitrary values were chosen for their utility in multilayer CPA/lasing modeling and to be consistent with previous studies by the authors in Ref. [37] and do not affect the conclusions drawn here.
- [32] M. Crescimanno, G. Mao, J. Andrews, K. Singer, E. Baer, A. Hiltner, H. Song, K. Comeau, B. Shakya, A. Bishop, and R. Livingston, *J. Opt. Soc. Am. B* **29**, 1038 (2012).
- [33] J. P. Dowling, M. Scalora, M. J. Bloemer, and C. M. Dowden, *J. Appl. Phys.* **75**, 1896 (1994).
- [34] J. H. Andrews, M. Crescimanno, K. D. Singer, and E. Baer, *J. Poly. Sci. B: Poly. Phys.* **52**, 251 (2014).
- [35] Y. Wu, K. D. Singer, R. G. Petschek, H. Song, E. Baer, and A. Hiltner, *Opt. Express* **17**, 18038 (2009).
- [36] E. Yablonovitch, *Phys. Rev. Lett.* **58**, 2059 (1987).
- [37] J. H. Andrews, M. Crescimanno, N. J. Dawson, G. Mao, J. B. Petrus, K. D. Singer, E. Baer, and H. Song, *Opt. Express* **20**, 15580 (2012).
- [38] M. Kang, F. Liu, and J. Li, *Phys. Rev. A* **87**, 053824 (2013).
- [39] In CPR, parity is not broken explicitly by the magnetic field (a psuedo-vector) itself.